

Soft Geometric Inductive Bias for Object Centric Dynamics

Hampus Linander¹Conor Heins¹Alexander Tschantz^{1,2}Marco Perin¹Christopher L Buckley^{1,2}¹VERSES AI²University of Sussex, Department of Informatics

{hampus.linander, conor.heins}@verses.ai

Abstract

Equivariance is a powerful prior for learning physical dynamics, yet exact group equivariance can degrade performance if the symmetries are broken. We propose object-centric world models built with geometric algebra neural networks, providing a soft geometric inductive bias. Our models are evaluated using simulated environments of 2d rigid body dynamics with static obstacles, where we train for next-step predictions autoregressively. For long-horizon rollouts we show that the soft inductive bias of our models results in better performance in terms of physical fidelity compared to non-equivariant baseline models. The approach complements recent soft-equivariance ideas and aligns with the view that simple, well-chosen priors can yield robust generalization. These results suggest that geometric algebra offers an effective middle ground between hand-crafted physics and unstructured deep nets, delivering sample-efficient dynamics models for multi-object scenes.

Code: <https://github.com/VersesTech/soft-geometric-inductive-bias>

1. Introduction

Learning world models that generalize far beyond their training distribution remains a central goal in machine learning, especially in applications for computer vision and robotics. Architectural priors—for example, weight sharing or equivariance to geometric transformations—can dramatically improve data efficiency and generalization [3]. At the same time, hard constraints can become liabilities when the underlying symmetries are only approximate, as is common in real environments with boundaries, contact events, anisotropic friction, damping, and actuation. This tension motivates *soft inductive biases*: parameterizations that nudge learning toward symmetry-respecting solutions while preserving headroom to fit structured violations of those symmetries [8, 31].

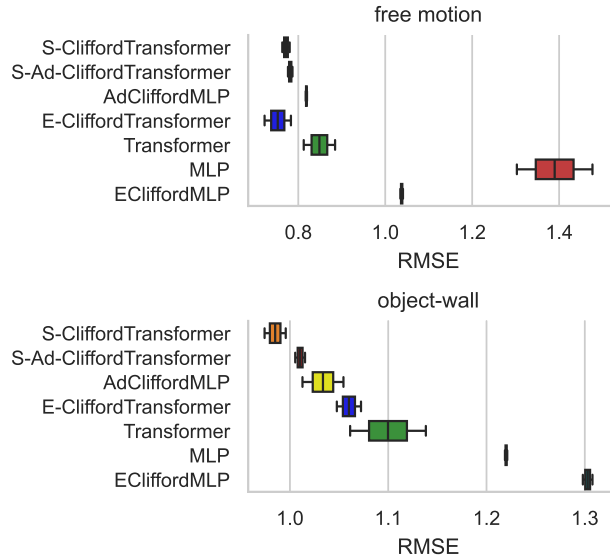


Figure 1. RMSE over 10 rollout frames against ground truth environment of 10 rigid body polygons colliding in a box with gravity, separated by free motion (top) and object-wall collisions (bottom). Our Clifford models with soft geometric inductive bias ($\{\mathbf{S}, \mathbf{S-Ad}\}$ -CliffordTransformer) outperforms the equivariant models as well as baseline transformers for the sparse object-wall collisions, while staying on-par with the best equivariant model (E-CliffordTransformer) during free motion.

World models of objects moving in space are a natural substrate for such priors. By factoring scenes into entities and interactions, they promise compositional generalization and long-horizon stability [21, 32]. Yet, learning *dynamics* (not just static properties) in multi-object scenes is brittle: contacts and constraints create sharp, state-dependent symmetry breaking, and naive, non-geometric architectures either overfit or require large data budgets. Conversely, strictly equivariant models can underfit when the data deviate from the assumed symmetries.

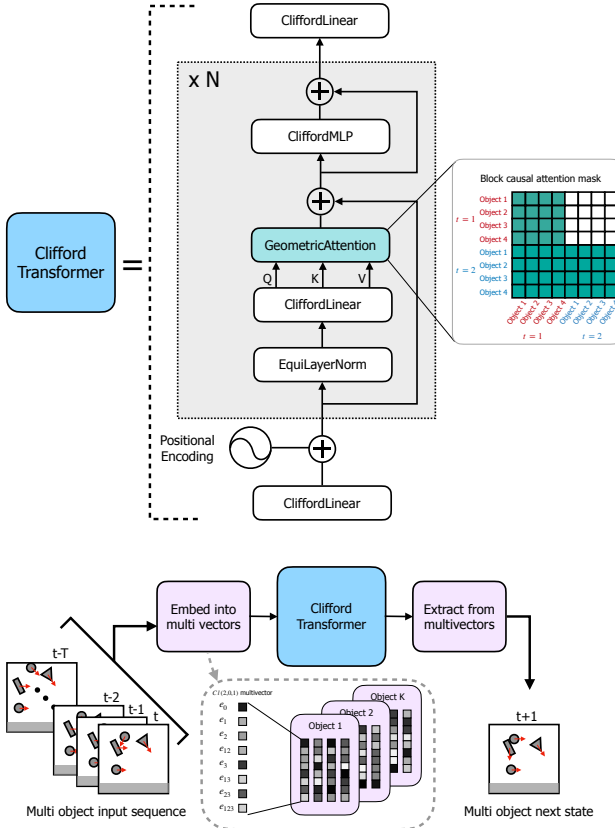


Figure 2. Top: Architecture diagram with the structure of N -block soft Clifford transformer models, including a block causal attention mask at the geometric attention layer. The block causal attention mask is shown for an example of 4 objects and two timesteps, making a total of $4 \times 2 = 8$ input tokens. Bottom: the flow of information from multi-object representations to predicted next states. This sequence of multi-object states on the left side indicates that we can condition the next multi-object state on a sequence of past states.

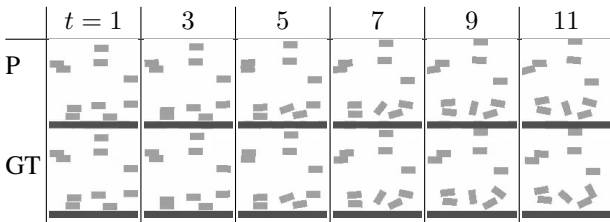


Figure 3. Example rollout of ground truth (bottom) and model prediction (top) of frames 1 (left) to 11 (right) using our S-CliffordTransformer. The model predicts position, velocity, angle and angular velocity of the 10 rigid body polygons colliding with both the other dynamic bodies and the static environment with gravity.

We argue that *geometric algebra* (Clifford algebra) [26] offers an effective middle ground for injecting geometric

structure softly. By representing both states and operators as multivectors, projective geometric algebra (PGA) provides the model with a bias towards geometric transformations. The tensor nature of multivectors enables efficient implementation of standard modules such as linear maps, attention and nonlinearity [2, 27]. Instead of enforcing exact $E(2)$ -equivariance end-to-end, our models use this soft geometric inductive bias to enable effective learning in environments with broken equivariance [27, 31]. The result is an *object-centric dynamics model with soft geometric bias*: a next-step predictor trained autoregressively on object states and capable of generating long-horizon, physically-plausible rollouts.

Practically, we embed each entity’s position, velocity, and orientation as multivectors in $\text{PGA}(2) \cong Cl(2, 0, 1)$ and train Clifford neural networks with soft geometric bias to predict sequences of this embedded activity. We train our architectures as dynamics models (i.e., on next-step prediction) on procedurally generated 2D rigid-body scenarios built with the JAX-based JAX2D engine [22]. We show that the soft geometric bias improves both sample efficiency and long-horizon physical fidelity relative to (i) non-geometric MLP/Transformer baselines and (ii) a strictly equivariant variant of the Clifford transformer.

This perspective complements recent arguments that much of deep learning’s generalization can be understood through the lens of explicit priors and parameterization choices [31], and it operationalizes “soft equivariance” ideas developed in residual pathway priors and related regularization schemes [8, 16]. It also connects to the emerging use of geometric algebra transformers across domains (e.g., $E(3)$ and Lorentz symmetry) which show that Clifford representations can unify objects and transformations within scalable attention architectures [2, 29].

Our main contributions are:

- **Object-centric dynamics with soft geometric bias.** We introduce a Clifford-based dynamics model that biases features and interactions toward $E(2)$ -consistent behavior while allowing controlled symmetry violations, yielding robustness in scenes with contacts, boundaries, and heterogeneous materials.
- **Autoregressive world modeling.** We train a geometrically-informed transition model with a next-token prediction objective and evaluate long-horizon rollouts in multi-object scenes. The model is trained with a block-causal teacher forcing objective that has not been used in object-centric dynamics modeling before.
- **Empirical gains on procedurally generated physics.** On JAX2D rigid-body environments, our models achieve lower rollout errors and higher sample efficiency than non-equivariant baselines, and outperform or match a strictly equivariant Clifford counterpart when symmetries

are only approximate.

2. Related work

Soft inductive biases. Existing work has explored the tension between restricting the solution space of deep neural networks with inductive biases like equivariance, and ‘softly’ parameterizing these biases to accommodate cases when the symmetries assumed by those biases are broken in the data distribution [13, 23–25, 31]. For example, Residual Pathway Priors convert hard constraints into priors that favor (but do not enforce) equivariance, improving robustness under misspecified symmetries [8]; related work regularizes toward mixed approximate symmetries [16], or specifically accommodates known violations of symmetries in otherwise equivariant models by modifying the input structure accordingly [29]. Wang et al. [30] learns to linearly combine a set of exactly equivariant kernels to relax equivariance constraints and identify broken symmetries. Our approach instantiates this philosophy with Clifford parameterizations for objects and interactions.

Equivariant architectures. Existing equivariant architectures include $SE(3)$ -Transformers and $E(n)$ -GNNs, which enforce exact geometric equivariances in attention and message passing [9, 28]. Geometric Algebra Transformers encode objects and operators in Clifford algebra with exact group equivariance in 3D or Lorentzian settings [2, 29]. Here, we develop a variant of the geometric algebra transformer that also adopts GA primitives, but without enforcing strict equivariance, targeting settings where symmetry is intermittent or approximate. Contemporary “efficient equivariant” Transformers (e.g., Platonic Transformers) similarly seek practical trade-offs between symmetry and flexibility [14].

Object-centric world models. This current work builds on existing literature on object-centric models, which decompose a high-dimensional sensory input (e.g., images or video) into exchangeable entities or objects, often referred to as ‘slots’ [4, 10, 21]. This decomposes the data into a modular and reusable set of slots, which helps such models excel in compositional generalization tasks, e.g., generalizing to scenes with unknown numbers and types of objects at test time [6]. Further work extends this to the time domain by putting autoregressive dynamics onto the slot representations, which can be useful for identifying objects in the first place [15] as well as for video prediction and planning [7, 12, 17–19, 32]. In our setting, we assume we already have object-centric ‘slots’ as inputs, but represent slot features in a projective geometric algebra and inject geometric constraints into their dynamics through Clifford neural networks. This is similar in spirit to other approaches which imbue slot dynamics with symmetries [1] or an explicit physics simulator [15]. The seminal work introducing geometric algebra transformer (GATr) includes an 3-D n -

body prediction task, but is distinct in that their model is not a time-invariant transition model, but rather it is trained to predict final object states after a short period of integration from a stationary distribution of initial conditions [2]. Additionally, the systems modeled in previous work like [2] and [28] are truly equivariant systems, whereas in our work the presence of static, unrepresented objects like walls in the environment breaks strict equivariance when considering only the modeled, dynamic objects. An additional novelty of our work is the first use, to our knowledge, of block causal attention for object-centric modeling; previous work has used block-causal attention on encoded image patches as tokens, which don’t explicitly represent objects [5, 11, 20].

Benchmarks. We use the JAX2D engine to procedurally generate a set of rigid-body environments within constrained arenas, stressing models with approximate symmetries and contact dynamics [22]. We use the KINETIX package (which uses JAX2D as its underlying physics engine) for constructing our environments and extracting the environmental state in the form of distinct objects (using the provided SYMBOLIC ENTITY format).

3. Geometric Algebra

The projective geometric algebra $Cl(2, 0, 1)$ is spanned by 8 basis vectors $\{e_0, e_1, e_2, e_3, e_{12}, e_{13}, e_{23}, e_{123}\}$, often referred to as blades to disambiguate from the vector part of the multivectors [26]. The algebra is equipped with the geometric product, a bilinear product such that $e_i \star e_i = 1$ for $i \in \{1, 2\}$ and $e_3 \star e_3 = 0$ for the projective dimension. Together with the anti-commutation relation $e_i \star e_j = -e_j \star e_i$ for $i \neq j$, this completely specifies the structure constants of the algebra. When writing the geometric product between basis blades we will omit the explicit \star , in fact the higher order basis blades are themselves just short-hand for the geometric product of the rank 1 basis blades e_1, e_2 and e_3 .

The algebra acts on itself through the twisted adjoint action $g(x) = g^* \star x \star g^{-1}$, with the grade involution g^* defined on monomials by $(e_1 \dots e_k)^* = (-1)^k e_1 \dots e_k$ and extended by linearity to polynomials. Through the twisted adjoint action each basis vector e_i can be identified with reflections in an orthogonal plane. Using the Cartan–Dieudonné theorem this can be extended to all the rotations of the 2-dimensional Euclidean group $E(2)$.

Geometric entities like points, vectors and lines can be naturally embedded in the Clifford algebra, and their transformations under $E(2)$ by the twisted adjoint action. For example points can be represented by the grade 1 basis vectors, and vectors using the grade 2 basis vectors. A rotation by an angle θ is parametrized by the rotor $R = \cos(\theta/2) + \sin(\theta/2)e_{12}$ that acts on multivectors by $R^* \star (xe_1 + ye_2) \star R^{-1}$, resulting in the rotated coordinates $(\cos(\theta)x - \sin(\theta)y)e_1 + (\sin(\theta)x + \cos(\theta)y)e_2$. In terms

of numerical tensors, a multivector in $Cl(2, 0, 1)$ will thus be an 8-dimensional real vector.

The geometric product between two multivectors can be calculated using the structure coefficients, i.e. the geometric product between the basis vectors, and using the linearity of the product.

$$x \star y = (x^i e_i) \star (y^j e_j) \quad (1)$$

$$= x^i y^j (e_i \star e_j) \quad (2)$$

$$= x^i y^j f_{ij}^k e_k, \quad (3)$$

where the indices i and j range over the set of 8 multivector dimensions $\{0, 1, 2, 3, 12, 13, 23, 123\}$ of $Cl(2, 0, 1)$, and f_{ij}^k are the structure constants

$$f_{ij}^k = (e_i \star e_j)^k \quad (4)$$

3.1. Implementation

The structure constants f_{ij}^k of equation (4) can be precalculated for $Cl(2, 0, 1)$ as a tensor f of shape $(8, 8, 8)$. Two multivectors x and y , represented by their 8 components, can then be multiplied with

```
def clifford_product(x, y, f):
    return einsum("...i,...j,ijk->...k",
                 x, y, f)
```

where f is the precomputed tensor containing the $8 \times 8 \times 8$ structure constants.

4. Clifford transformer

Using the geometric algebra primitives we implement a transformer architecture that acts on a multiple entities per timestep, where each entity is represented by C multivectors.

4.1. Embedding

The position of the center of mass, as well as the position of polygon vertices, are embedded as multivectors using the e_{13} and e_{23} basis vectors. The velocity of objects are embedded using e_1 and e_2 . Rotational angle, as well as angular velocity, is embedded using rotors $\cos(\theta) + \sin(\theta)e_{12}$. Each of these quantities is thus embedded as a separate multivector so that for example a circle with center of mass position (x, y) , velocity (vx, vy) , rotation angle θ and angular velocity $\dot{\theta}$, is represented as four multivectors

$$v_1 = xe_{13} + ye_{23} \quad (5)$$

$$v_2 = vx e_1 + vy e_2 \quad (6)$$

$$v_3 = \cos(\theta) + \sin(\theta)e_{12} \quad (7)$$

$$v_4 = \cos(\dot{\theta}) + \sin(\dot{\theta})e_{12}. \quad (8)$$

This will correspond to one token in the input sequence where we view the 4 multivectors as 4 channels, each with 8 multivector components. A sequence of such tokens (for one object) is thus of the shape $(T, C, 8)$ where T is the sequence dimension and C is the multivector channel count. In the case of K different objects we have an input sequence of shape $(T, K, C, 8)$, which represents the sequence of each object's multivector tokens over time. In Sec. 4.4 we describe how we deal with the T and K dimensions jointly during the attention operation.

4.2. Clifford MLP

Using the building blocks of the geometric algebra, an extension of a standard linear layer can be constructed using multivector weights and features

$$S(x) = W^{ij} \star x_j, \quad (9)$$

where W is the learnable weight matrix with multivector coefficients, and $x = (x_1, x_2, \dots, x_n)$ with $x_i \in Cl(2, 0, 1)$ is a collection of multivectors.

For non-linear activation $a(x)$ we use a gated sigmoid

$$a(x) = \sigma(W_i^{\text{act}} x^i) x. \quad (10)$$

A Clifford multilayer perceptron (CMLP) can then be constructed with the notation (n_1, n_2, \dots, n_N) corresponding to N linear layers followed by gated sigmoid activation after all but the last layer.

We also evaluate models with adjoint linear layers where the multivector weights acts through the adjoint sandwich product. To simplify the implementation we follow prior work [27] and use the Clifford reverse instead of the Clifford inverse.

$$S_{\text{Ad}}(x) = W^{ij} \star x_j \star (W^{ij})^r \quad (11)$$

where $(\cdot)^r$ is the Clifford reverse.

4.3. Geometric algebra attention

Following [2], we use one of the natural induced inner products on $Cl(2, 0, 1)$ to implement multi-head attention. Explicitly, the inner product between two multivectors $x = x_0 + x_1 e_1 + \dots + x_{123} e_{123}$ and $y = y_0 + y_1 e_1 + \dots + y_{123} e_{123}$ takes the form

$$x \cdot y = x_0 y_0 + x_1 y_1 + x_2 y_2 + x_{12} y_{12}, \quad (12)$$

with no contribution from the projective basis vector e_3 .

Using three linear layers Q, K, V , self-attention is implemented with

$$\text{att}(x) = \text{softmax}_j (Q(x)_i \cdot K(x)_j) V(x)_j, \quad (13)$$

where Q, K, V output multivectors.

4.4. Architecture

We use three main variations of a transformer based on the Clifford primitives. The different versions use three different implementations of the MLP used throughout the model. The first uses a Clifford MLP as described in section 4.2, referred to as `S-CliffordTransformer`, giving a soft geometric inductive bias. The second uses a linear layer where the multivector weights act on the input by the adjoint map, referred to as `S-Ad-CliffordTransformer`, giving a soft inductive bias with the ability to directly parametrize a geometric transformation. The third is an exactly equivariant model using an equivariant linear map [2] with rank-wise linear combinations referred to as `E-CliffordTransformer`.

All transformer models are trained to perform sequence prediction using ‘teacher forcing’, where the previous $S - 1$ tokens are used to condition prediction of the S^{th} token. The Clifford transformers starts with an embedding of the object centric variables as multivectors, followed by a channel expansion using a linear layer into shape $(B, S, K, C, 8)$, corresponding to batch (B), sequence position (S), object index (K), multivector channel (C) and the 8 dimensions of $Cl(2, 0, 1)$. After channel expansion, we apply a sinusoidal positional embedding to the sequence position, adapted to the sequence lengths relevant for the task. After this, the sequence and object dimensions are flattened into a single $N = S \times K$ dimension leaving a tensor of shape $(B, N, C, 8)$. This means that each token for the subsequent attention operation represents an object at a particular sequence position.

This is followed by a number of attention blocks, where each block performs causal multi-head self attention (MHA).

$$\begin{aligned} z &= \text{CliffordMHA}(x) + x \\ y &= \text{CliffordMLP}(z) + z \end{aligned} \quad (14)$$

The multi-head attention uses the Clifford algebra attention from section 4.3, and a block-causal mask so that all objects at a given timestep are predicted in parallel rather than sequentially [5]. This also means that the model can reason jointly about all tokens within a given timestep when predicting the next timestep. In the case of generating rollouts in object-centric space, the Clifford transformers extract their outputs extraction into object-centric coordinates. When training these models, however, we compute and differentiate an L_2 loss directly in the predicted multivector space, without decoding back to object-centric variables.

See Table 1 for the transformer hyperparameters. For the baseline transformer we use exactly the same architecture, but with embedding dimension matched against total parameter count. See Appendix for further model ablations.

Blocks (B)	Heads (H)	MV (C)	N_p
10	8	24	1.5M

Table 1. Clifford transformers hyperparameters with number of multivector channel C and number of trainable parameters N_p .

4.5. Soft geometric bias

Through the use Clifford algebra primitives, our models are constructed to have a soft geometric inductive bias without enforcing strict equivariance. Other works, such as the Geometric Algebra Transformer (GATr) [2] target the equivariant domain by using only equivariant operations. Although the geometric algebra provides a natural framework for equivariant models, it also provides a succinct parametrization of non-equivariant geometric transformations. To see why this is, recall that given and input $x \in X$ in a space with an action of a group G , a function $f : X \rightarrow Y$ is said to be equivariant if $f(gx) = gf(x)$, where $g \in G$ acts through a possibly different representation on the output space Y . In other words, if the input transforms, the output should follow along.

Since the Clifford inner product is by definition invariant under the action of $E(2)$, the attention block transforms in the same representation as the value map $V(x)$. In this work, we evaluate three different ways of parameterizing the MLP that is used for all projections in the models: the exactly equivariant linear map of GATr using rank-wise linear combinations, a Clifford linear map $S(x)^i = w^{ij} \star x_j$ and a Clifford adjoint linear map $S_{\text{Ad}}(x)^i = w^{ij} \star x_j \star (w^{ij})^r$, where $(\cdot)^r$ denotes the reverse operation. Neither of these latter two linear maps are equivariant since the action of $E(2)$ on a multivector x parametrized by another multivector m is given by $m^r \star x \star m^{-1}$ and

$$S(m^r \star x \star m^{-1})^i = w^{ij} \star m^r \star x_j \star m^{-1} \quad (15)$$

$$\neq m^r \star w^{ij} \star x_j \star m^{-1} \quad (16)$$

$$= m^r \star S(x) \star m^{-1}, \quad (17)$$

by the non-commutativity of the geometric product. An almost identical computation shows this to be the case for S_{Ad} as well. As such, our models using the linear maps S and S_{Ad} have a soft geometric inductive bias without enforcing strict equivariance.

5. Dataset

We use the JAX2D engine [22] to flexibly configure 2D physics environments with a desired number of objects and physical properties.

All environments consists of dynamic rigid objects, either circles or rectangles, confined to a box and under the influence of gravity. The dynamic objects may collide with

each other and with the static walls of the box. In all environments we use a friction coefficient of 1.0 and a coefficient of restitution for the collisions of 1.0 apart from the surfaces of the static walls, which have a coefficient of restitution of 0.9. We find that the integration scheme of JAX2D can result in unstable simulation without the use of some damping. Although JAX2D environments contain also joints and thrusters, as well as possible actions, we only use rigid body circles and rectangles for our datasets.

We define a training dataset by sampling N episodes with 128 frames per episode. For our experiments we use $N = 100$ and $N = 1000$, resulting in 12800 frames and 128000 frames respectively. Each episode is reset with uniform random values for the different state variables of the objects.

6. Results

We train all models using a batchsize of 128, optimizing with AdamW using a learning rate of $5 \cdot 10^{-4}$. For the transformers and CliffordMLP we train with weight decay 10^{-7} and for the baseline MLP $3 \cdot 10^{-6}$. All models are trained using an L_2 loss, where we find it beneficial to train the Clifford models using the L_2 loss directly in multivector space.

6.1. Baselines

We evaluate against two baseline models without any geometric inductive bias: standard MLPs (MLP) and transformers (Transformer). The MLPs are two-layer ReLU activated with parameter-matched layer widths. The baseline transformer follows the same architecture as the Clifford transformer using standard inner-product attention and block causal masking on an embedding space with dimensions adapted to match the overall parameter count of the Clifford transformer. To separate the effect of geometric inductive bias from the transformer architecture, we also include Clifford MLPs using the Clifford geometric product and multivector weights.

6.2. Metrics

To assess the quality of the model prediction over a rollout of multiple frames we use a number of metrics starting with the rollout RMSE.

$$\text{RMSE}_N = \sqrt{\frac{1}{N \cdot N_{\text{vars}}} \sum_{t=0}^N \sum_{i \in \text{vars}} (y_t^i - \hat{y}_t^i)^2} \quad (18)$$

where N is the number of frames from the start of the sequence, y_t^i is the model prediction for variable i at time t , and \hat{y}_t^i is the target ground truth from the environment.

To separate the effect of accumulated errors from the models ability to correctly predict the forward integration

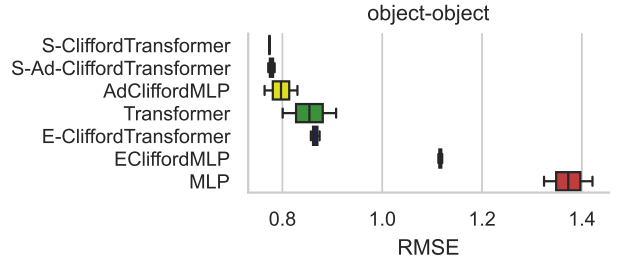


Figure 4. Rollout RMSE over 10 frames for object-object collision, complementing the two other modes illustrated in Figure 1. Models are ordered by their RMSE from best (S-CliffordTransformer) to worst (MLP).

of the physics, we also evaluate the deviation from one forward simulation of the state using the ground truth environment, giving a measure of the local dynamics error.

$$\text{RMSE}_N^{\text{Euler}} = \sqrt{\frac{1}{N \cdot N_{\text{vars}}} \sum_{t=0}^N \sum_{i \in \text{vars}} (y_t^i - \hat{y}_t^i)^2} \quad (19)$$

where y_t^i is the prediction at time t of variable i , and \hat{y}_t is one environment step from the predicted state y_{t-1} .

6.3. Experiments

In Figure 1, our models with soft geometric inductive bias are evaluated against a baseline transformer using the same number of blocks and heads with parameter matched embedding dimensions, as well as an exactly equivariant Clifford transformer. In the bottom panel, validation rollout RMSE is calculated over 10 frames for all dynamic variables (position, velocity, angle and angular velocity) for frames with object-wall collisions. Since information about the geometry of the wall is not encoded in the input, this presents a non-equivariant quantity that the models need to learn. Our soft models ($\{S, S\text{-Ad}\}\text{-CliffordTransformer}$, AdCliffordMLP) outperform the baseline transformer and exactly equivariant Clifford transformer in terms of rollout RMSE for these frames. On the other hand, the free motion dynamics is still mostly equivariant and here the equivariant $E\text{-CliffordModel}$ has the lowest RMSE, but our soft models still perform on-par. Figure 4 contains the 10 frame rollout RMSE for the remaining frame type of object-object interactions complementing the free motion and object-wall types in Figure 1. Our $\{S, S\text{-Ad}\}\text{-CliffordTransformer}$ outperforms both the equivariant and the transformer baseline. An example of predicted frames from a rollout compared to ground truth simulation can be seen in Figure 3.

We evaluate long-horizon rollout performance by RMSE of up to 35 frames. In Figure 6, the rollout RMSE of our models compared to baselines are shown for sequence length 1, i.e. all models are performing next-frame predictions using only the dynamic variables from the current frame as input. The best performing model at 35 frames is our S-Ad-CliffordTransformer. The baseline MLP struggles to generalize, as well as the exactly equivariant Clifford MLP. The baseline transformer does learn some features of the dynamics, but there is growing gap in total RMSE for longer horizons. In terms of the total RMSE, the equivariant transformer is doing well on account of its good performance on free motion frames as evidenced by the free motion panel in Figure 1. For longer horizons, S-Ad-CliffordTransformer surpasses the equivariant model also in terms of total RMSE.

Longer sequence context can be beneficial to dynamics models, and to evaluate how this affects performance we evaluate all transformer-based models first using 2 input frames with block causal attention. Figure 7 shows the rollout RMSE for all transformer models trained on 10k frames of 10 rigid body polygons. With the additional context of 2 frames, the baseline transformer matches performance of the soft and exactly equivariant models for shorter rollout lengths, but there is again a significant gap at longer rollouts. We also investigate the scaling behavior of the sequence length and dataset size by also including sequence length 16 and $N = 1000$ episode results in Figure 5, where our $\{\text{S, S-Ad}\}$ -CliffordTransformer models still outperform the baseline transformer.

To further resolve how the soft inductive biases helps generalization, we evaluate the RMSE of next frame predictions against the environment ground truth forward step at each point along a long-horizon rollout. Figure 8 left panel shows the RMSE for one component $\sin(\theta)$ of the rotor prediction, i.e. the angular orientation of the polygons, on frames of object-object interactions. As object-object interactions are equivariant under $\text{SE}(2)$ we expect the exactly equivariant models to perform well, which is reflected in the second best Euler RMSE after the soft Clifford transformer. For object-wall type interactions in Figure 8 right panel, the soft Clifford models perform better than the exactly equivariant model. This is again expected given the non-equivariance introduced by the static walls that are not part of the multi-object state provided to the models.

We also evaluate on environments with both polygons and discs. This means that the models have to learn non-trivial association of different moments on inertia and the effect of collision point on the resulting momentum and angular momentum. Figure 9 shows the total rollout RMSE over 20 frames for models trained on 10k frames using an input sequence length of 2. Note that this is twice as long as the rollout horizon in Figure 1. Between the Clifford

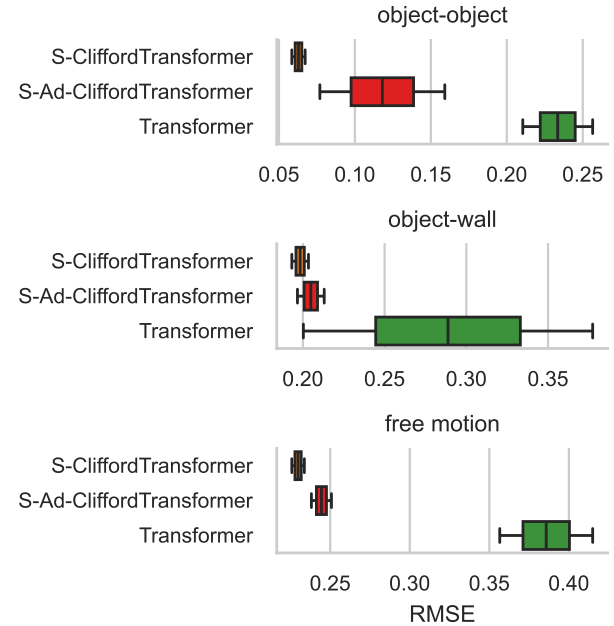


Figure 5. Rollout RMSE for transformer models with sequence length 16 and $N = 1000$ episodes of 4 rigid body circles. Our models still outperform the baseline transformer in this regime, and attain significantly lower rollout error.

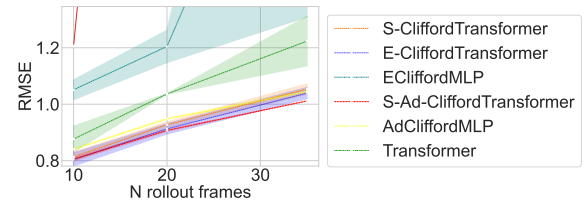


Figure 6. Long-horizon rollout RMSE for models trained on 10k frames with sequence length 1. All transformer models use the L architecture with 10-block, see section 4.4. Colored bands indicate 95% CI intervals.

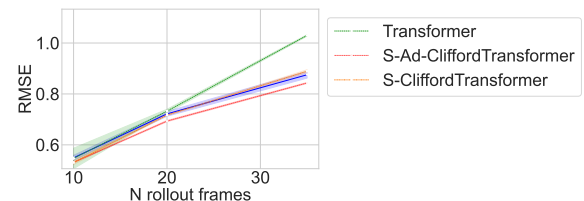


Figure 7. Rollout RMSE for models trained on 10k frames. All transformer models use a 10-block architecture with a causal sequence length of 2. With the additional context, the baseline transformer at this model scale can reach overall RMSE comparable to the our $\{\text{S, S-Ad}\}$ -CliffordTransformer for shorter sequence lengths.

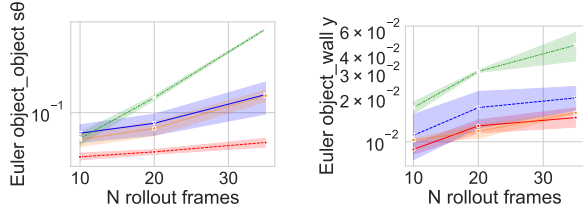


Figure 8. Euler RMSE for $\sin(\theta)$ on frames of object-object collisions (left) and y on frames of object-wall interactions (right) for models trained on 10k frames. Colors indicate Transformer (green), E-CliffordTransformer (blue) and $\{\mathcal{S}, \mathcal{S}\text{-Ad}\}$ -CliffordTransformer (orange and red).

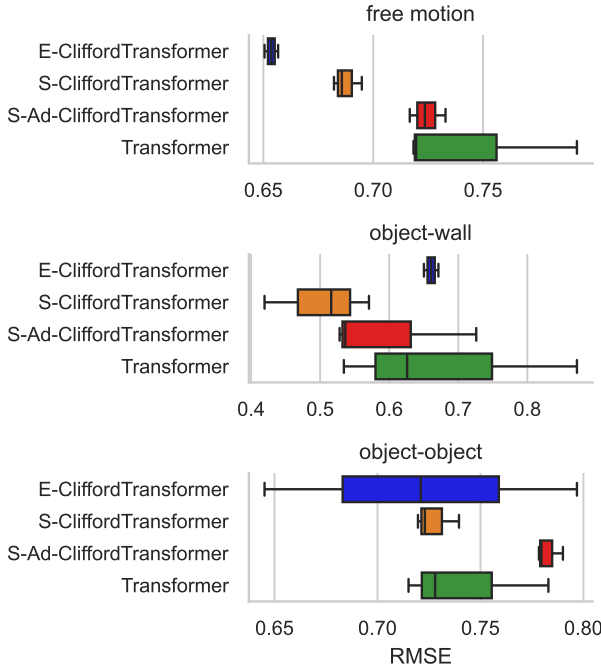


Figure 9. Rollout RMSE for 10 frames separated by frame type for all predicted variables. All models use input sequences of 2 frames and are trained using 10k simulated frames of 6 rigid body circles and 4 rigid body polygons.

based transformers, the trend observed for the 10 polygon case in Figure 1 persists. For free motion frames, the equivariant E-CliffordTransformer has lower RMSE, whereas for interactions with other objects and static environment our $\{\mathcal{S}, \mathcal{S}\text{-Ad}\}$ -CliffordTransformer performs better. At this longer rollout horizon the gap to the baseline transformer is increasing.

6.4. Sample efficiency

To measure the sample efficiency of the models we compare the number of epochs needed to match the minimum rollout RMSE of the baseline transformer. Figure 11 shows that the

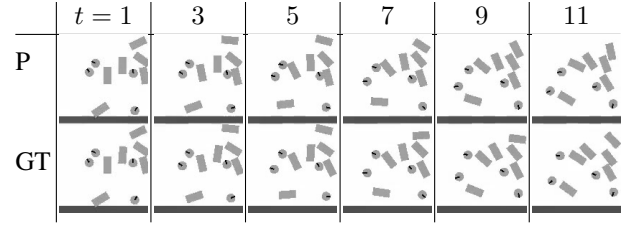


Figure 10. Example rollout of ground truth (bottom) and model prediction (top) of frames 1 (left), 3, 5, 7, 9, 11 (right) using our S-CliffordTransformer. The model predicts position, velocity, angle and angular velocity of the 6 rigid body discs and 4 polygons colliding with both the other dynamic bodies and the static environment under the influence of gravity.

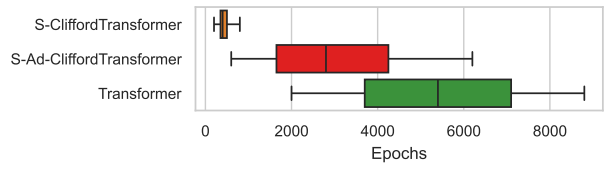


Figure 11. Epochs to match baseline transformer rollout RMSE at 10 frames. Models trained with sequence length 16 and $N = 1000$ episodes.

soft inductive bias of the S-CliffordTransformer quickly captures the dynamics of the environment compared to the baseline transformer.

7. Conclusions

We introduced object-centric dynamics models with soft geometric bias through the use of geometric algebra primitives. Our soft Clifford transformers are simple to implement, and outperform exactly equivariant models as well as non-equivariant transformer baselines when trained to predict the dynamics of rigid body systems with broken equivariance through static objects and constant forces. In free-motion regimes the strictly equivariant model remains competitive, but during symmetry-breaking interactions our soft parameterizations maintain lower rollout error and reduced local dynamics error, indicating a better learned flow field. Importantly, because we train these models autoregressively as next-step predictors, the networks can roll out physically-realistic trajectories over long horizons without being restrained to exact equivariance. This suggests the potential use of soft Clifford transformers as transition models in object-centric world models [7, 19]. We hope that this paves the way for further use of soft geometric inductive bias as an effective tool to model real world data distributions where symmetries are often approximate.

References

[1] Bahar Azari and Deniz Erdogmus. Equivariant deep dynamical model for motion prediction. In *International Conference on Artificial Intelligence and Statistics*, pages 11655–11668. PMLR, 2022. 3

[2] Johann Brehmer, Pim De Haan, Sönke Behrends, and Taco S Cohen. Geometric algebra transformer. *NeurIPS*, 36:35472–35496, 2023. 2, 3, 4, 5

[3] Johann Brehmer, Sönke Behrends, Pim De Haan, and Taco Cohen. Does equivariance matter at scale? *Transactions on Machine Learning Research*, 2025. 1

[4] Christopher P Burgess, Loic Matthey, Nicholas Watters, Rishabh Kabra, Irina Higgins, Matt Botvinick, and Alexander Lerchner. Monet: Unsupervised scene decomposition and representation. *arXiv preprint arXiv:1901.11390*, 2019. 3

[5] Antoine Dedieu, Joseph Ortiz, Xinghua Lou, Carter Wendelken, Wolfgang Lehrach, J Swaroop Guntupalli, Miguel Lazaro-Gredilla, and Kevin Patrick Murphy. Improving transformer world models for data-efficient rl. *arXiv preprint arXiv:2502.01591*, 2025. 3, 5

[6] SM Eslami, Nicolas Heess, Theophane Weber, Yuval Tassa, David Szepesvari, Geoffrey E Hinton, et al. Attend, infer, repeat: Fast scene understanding with generative models. *Advances in neural information processing systems*, 29, 2016. 3

[7] Stefano Ferraro, Pietro Mazzaglia, Tim Verbelen, and Bart Dhoedt. Focus: object-centric world models for robotic manipulation. *Frontiers in Neurorobotics*, 19:1585386, 2025. 3, 8

[8] Marc Finzi, Gregory Benton, and Andrew G Wilson. Residual pathway priors for soft equivariance constraints. *NeurIPS*, 34:30037–30049, 2021. 1, 2, 3

[9] Fabian Fuchs, Daniel Worrall, Volker Fischer, and Max Welling. Se (3)-transformers: 3d roto-translation equivariant attention networks. *NeurIPS*, 33:1970–1981, 2020. 3

[10] Klaus Greff, Raphaël Lopez Kaufman, Rishabh Kabra, Nick Watters, Christopher Burgess, Daniel Zoran, Loic Matthey, Matthew Botvinick, and Alexander Lerchner. Multi-object representation learning with iterative variational inference. In *International conference on machine learning*, pages 2424–2433. PMLR, 2019. 3

[11] Danijar Hafner, Wilson Yan, and Timothy Lillicrap. Training agents inside of scalable world models. *arXiv preprint arXiv:2509.24527*, 2025. 3

[12] Conor Heins, Toon Van de Maele, Alexander Tschantz, Hampus Linander, Dimitrije Markovic, Tommaso Salvatori, Corrado Pezzato, Ozan Catal, Ran Wei, Magnus Koudahl, et al. Axiom: Learning to play games in minutes with expanding object-centric models. *arXiv preprint arXiv:2505.24784*, 2025. 3

[13] Ningyuan Huang, Ron Levie, and Soledad Villar. Approximately equivariant graph networks. *Advances in Neural Information Processing Systems*, 36:34627–34660, 2023. 3

[14] Mohammad Mohaiminul Islam, Rishabh Anand, David R Wessels, Friso de Kruiff, Thijs P Kuipers, Rex Ying, Clara I Sánchez, Sharvaree Vadgama, Georg Bökman, and Erik J Bekkers. Platonic transformers: A solid choice for equivariance. *arXiv preprint arXiv:2510.03511*, 2025. 3

[15] Miguel Jaques, Michael Burke, and Timothy Hospedales. Physics-as-inverse-graphics: Unsupervised physical parameter estimation from video. *arXiv preprint arXiv:1905.11169*, 2019. 3

[16] Hyunsu Kim, Hyungi Lee, Hongseok Yang, and Juho Lee. Regularizing towards soft equivariance under mixed symmetries. pages 16712–16727. PMLR, 2023. 2, 3

[17] Thomas Kipf, Elise Van der Pol, and Max Welling. Contrastive learning of structured world models. *arXiv preprint arXiv:1911.12247*, 2019. 3

[18] Adam Kosiorek, Hyunjik Kim, Yee Whye Teh, and Ingmar Posner. Sequential attend, infer, repeat: Generative modelling of moving objects. *Advances in Neural Information Processing Systems*, 31, 2018.

[19] Jannik Kossen, Karl Stelzner, Marcel Hüssing, Claas Voelcker, and Kristian Kersting. Structured object-aware physics prediction for video modeling and planning. *arXiv preprint arXiv:1910.02425*, 2019. 3, 8

[20] Yuxuan Liu, Jingmin Sun, and Hayden Schaeffer. Bcat: A block causal transformer for pde foundation models for fluid dynamics. *arXiv preprint arXiv:2501.18972*, 2025. 3

[21] Francesco Locatello, Dirk Weissenborn, Thomas Unterthiner, Aravindh Mahendran, Georg Heigold, Jakob Uszkoreit, Alexey Dosovitskiy, and Thomas Kipf. Object-centric learning with slot attention. *NeurIPS*, 33:11525–11538, 2020. 1, 3

[22] Michael Matthews, Michael Beukman, Chris Lu, and Jakob Foerster. Kinetix: Investigating the training of general agents through open-ended physics-based control tasks. *arXiv preprint arXiv:2410.23208*, 2024. 2, 3, 5

[23] Daniel McNeela. Almost equivariance via lie algebra convolutions. *arXiv preprint arXiv:2310.13164*, 2023. 3

[24] Jung Yeon Park, Sujay Bhatt, Sihan Zeng, Lawson LS Wong, Alec Koppel, Sumitra Ganesh, and Robin Walters. Approximate equivariance in reinforcement learning. *arXiv preprint arXiv:2411.04225*, 2024.

[25] Mircea Petrache and Shubhendu Trivedi. Approximation-generalization trade-offs under (approximate) group equivariance. *Advances in Neural Information Processing Systems*, 36:61936–61959, 2023. 3

[26] Martin Roelfs and Steven De Keninck. Graded symmetry groups: plane and simple. *Advances in Applied Clifford Algebras*, 33(3):30, 2023. 2, 3

[27] David Ruhe, Johannes Brandstetter, and Patrick Forré. Clifford group equivariant neural networks. *NeurIPS*, 36:62922–62990, 2023. 2, 4

[28] Victor Garcia Satorras, Emiel Hoogeboom, and Max Welling. E (n) equivariant graph neural networks. pages 9323–9332. PMLR, 2021. 3

[29] Jonas Spinner, Victor Bresò, Pim De Haan, Tilman Plehn, Jesse Thaler, and Johann Brehmer. Lorentz-equivariant geometric algebra transformers for high-energy physics. *NeurIPS*, 37:22178–22205, 2024. 2, 3

[30] Rui Wang, Robin Walters, and Rose Yu. Approximately equivariant networks for imperfectly symmetric dynamics.

In *International Conference on Machine Learning*, pages 23078–23091. PMLR, 2022. [3](#)

- [31] Andrew Gordon Wilson. Deep learning is not so mysterious or different. *arXiv preprint arXiv:2503.02113*, 2025. [1](#), [2](#), [3](#)
- [32] Ziyi Wu, Nikita Dvornik, Klaus Greff, Thomas Kipf, and Animesh Garg. Slotformer: Unsupervised visual dynamics simulation with object-centric models. *arXiv preprint arXiv:2210.05861*, 2022. [1](#), [3](#)

Soft Geometric Inductive Bias for Object Centric Dynamics

Supplementary Material

8. Model ablations

To select the main architecture hyperparameters (number of blocks, number of heads, number of internal channels) we performed a number of ablations for both our $\{\mathbf{S}, \mathbf{S}\text{-Ad}\}$ -CliffordTransformer models and for the baseline Transformer. After an initial exploration phase we identified favorable regions for these three hyperparameters. First, for number of blocks in Figure 12, both our models and the baseline transformer are stable under our training schedule up to 10 blocks, and our CliffordTransformer models continue to show stable training at 20 blocks. In terms of rollout RMSE, the baseline transformer performs best at 10 blocks which is the value chosen for all the main experiments. Second, for number of transformer heads in Figure 13 we again find a similar pattern, with the baseline transformer having a preferred value of 8 heads among the ablated values. Again, we choose this favorable point for the baseline transformer as the value used for all the main experiments. Third, for the internal channel counts we do a separate ablation starting from a parameter matched point. Since the Clifford-based transformers have more parameters per channel on account of the 8 multivector dimensions, we cannot simply match the overall channel count. Similarly to the other main hyperparameters, we choose 64 channels as a point where the baseline transformer performs well here and then we parameter match our CliffordTransformer models at this point resulting in 24 multivector channels. See Figure 14 and 15 for channel ablations. In summary, the overall architecture hyperparameters resulting from this ablation for our CliffordTransformer models are shown in Table 1 in the main manuscript.

9. Qualitative results

We also include a number of qualitative results in the form of rollouts from an initial environment state for environments with 10 circles, 4 circles, 2 circles and 2 rectangles and 10 rectangles. The rollouts are chosen to highlight the typical behavior of the models over many rollouts.

Starting with the 10 circles environment, Figure 16 shows a rollout using the baseline Transformer, and Figure 17 using our $\mathbf{S}\text{-Ad}$ -CliffordTransformer. Note that the baseline predictions results in static object penetration, e.g. starting at timestep 7. Furthermore, while our Clifford transformer in Figure 17 does a robust rollout with good qualitative agreement up to timestep 20, and rough agreement all the way up to timestep 49, the baseline transformer quickly diverges.

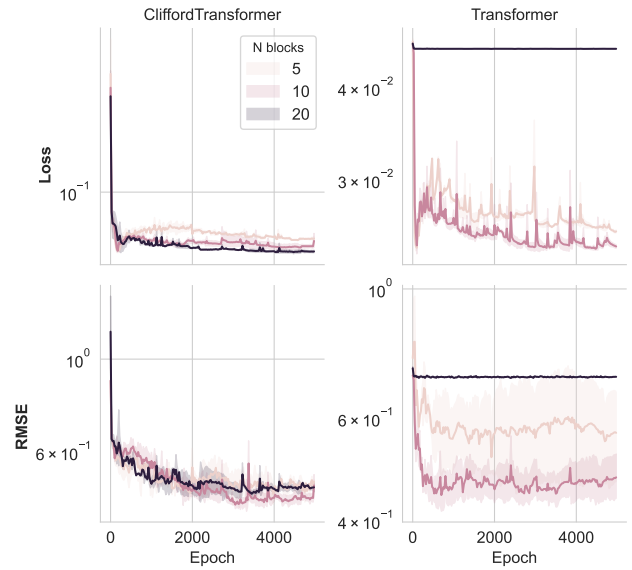


Figure 12. Validation loss and 10 frame rollout RMSE during training for different number of transformer blocks (5, 10, 20) for our $\{\mathbf{S}, \mathbf{S}\text{-Ad}\}$ -CliffordTransformer models and baseline Transformer. Trained on 100 episodes with sequence length of 16.

Continuing with 4 circles, our Clifford transformer in Figure 19 captures the dynamics almost perfectly up to timestep 28 where a collision occurs. The collision is detected and resolved, although slightly different from the ground truth environment. In contrast, the baseline transformer in Figure 18 fails to predict the free motion dynamics such that the collision occurs at all.

Finally, for the more challenging task of predicting the dynamics of 10 rectangles, we compare Equi-CliffordTransformer, S-CliffordTransformer and baseline Transformer in Figures 20, 21, 22. Our S-CliffordTransformer in Figure 21 shows rough qualitative agreement with ground truth up to timestep 28, but the predicted objects tend to dissipate energy more quickly than their ground truth counterparts. The Equi-CliffordTransformer also shows rough qualitative agreement, but note that sometimes there are predicted penetrations between dynamic and static objects in early timesteps such as in timestep 8. The baseline transformer in Figure 22 quickly diverges, failing to restrict the dynamic objects within the confines of the learned static environment.

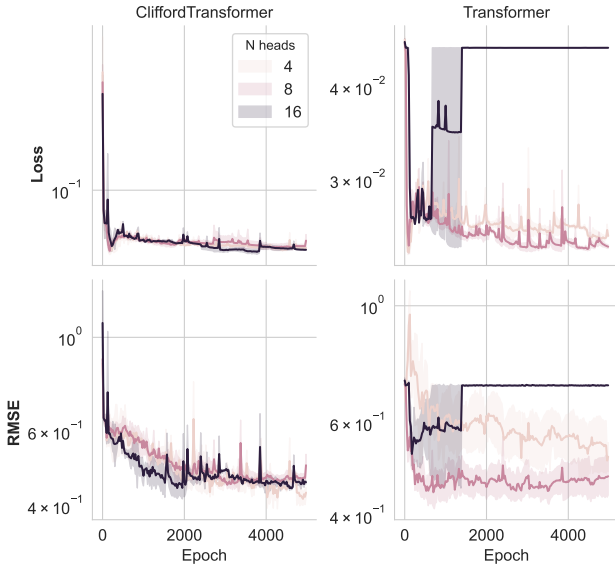


Figure 13. Validation loss and 10 frame rollout RMSE during training for different number of transformer heads (4, 8, 16) for our $\{\mathbf{S}, \mathbf{S-Ad}\}$ -CliffordTransformer models and baseline Transformer. Trained on 100 episodes with sequence length of 16.

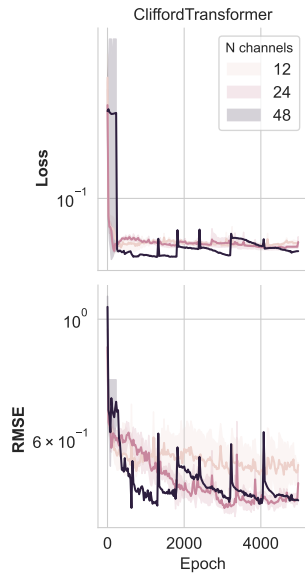


Figure 14. Validation loss and 10 frame rollout RMSE during training for different number of multivector channels (12, 24, 48) for our $\{\mathbf{S}, \mathbf{S-Ad}\}$ -CliffordTransformer models. Trained on 100 episodes with sequence length of 16.

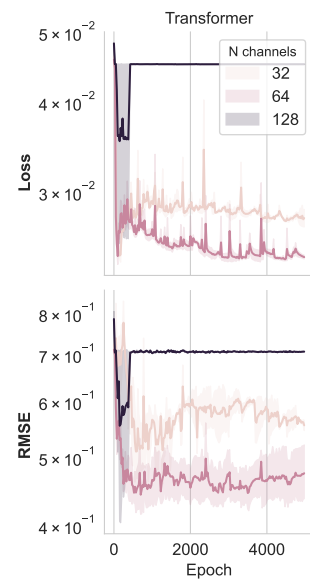


Figure 15. Validation loss and 10 frame rollout RMSE during training for different embedding dimensions (32, 64, 128) for the baseline Transformer. Trained on 100 episodes with sequence length of 16.

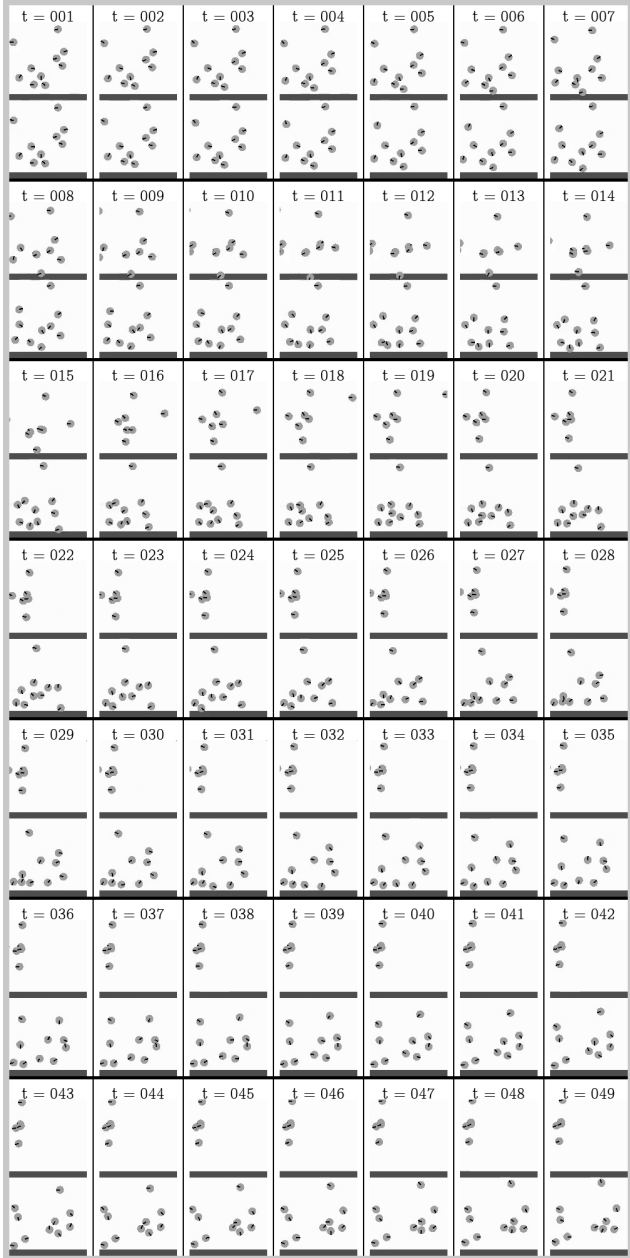


Figure 16. Example rollout using baseline transformer trained on 1000 episodes of 10 circles using sequence length 16. For each timestep, model prediction is shown in the top panel, and the ground truth environment simulation in the bottom panel.

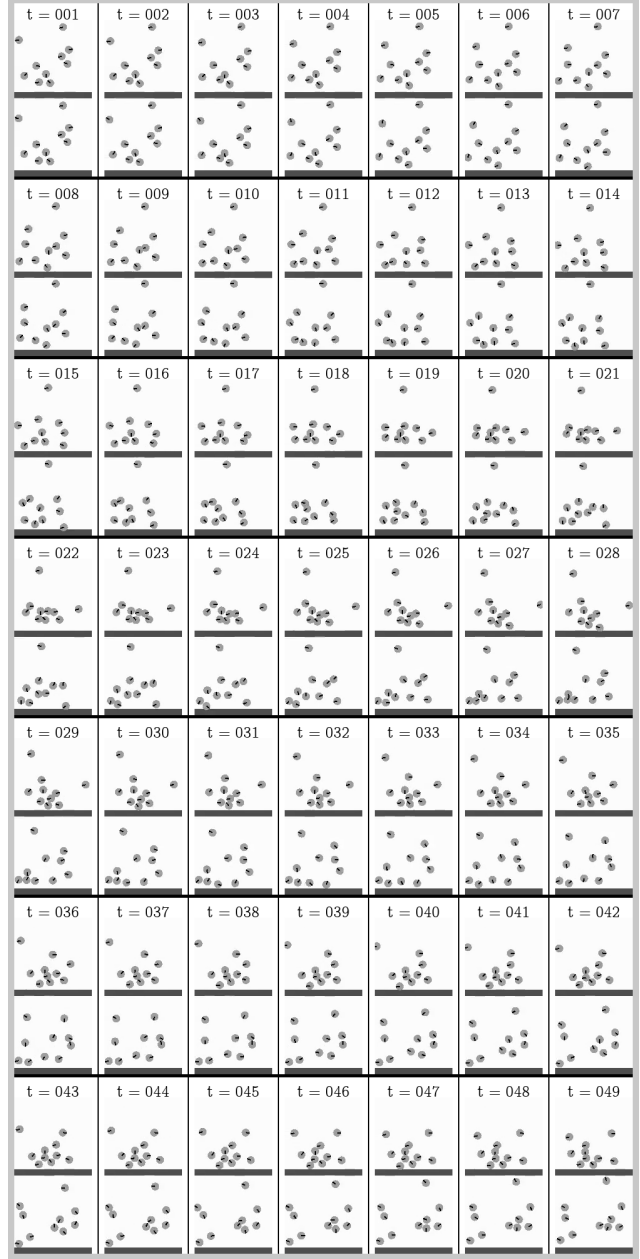


Figure 17. Example rollout using S-Ad-CliffordTransformer, using adjoint linear layers, trained on 1000 episodes of 10 circles using sequence length 16. For each timestep, model prediction is shown in the top panel, and the ground truth environment simulation in the bottom panel.

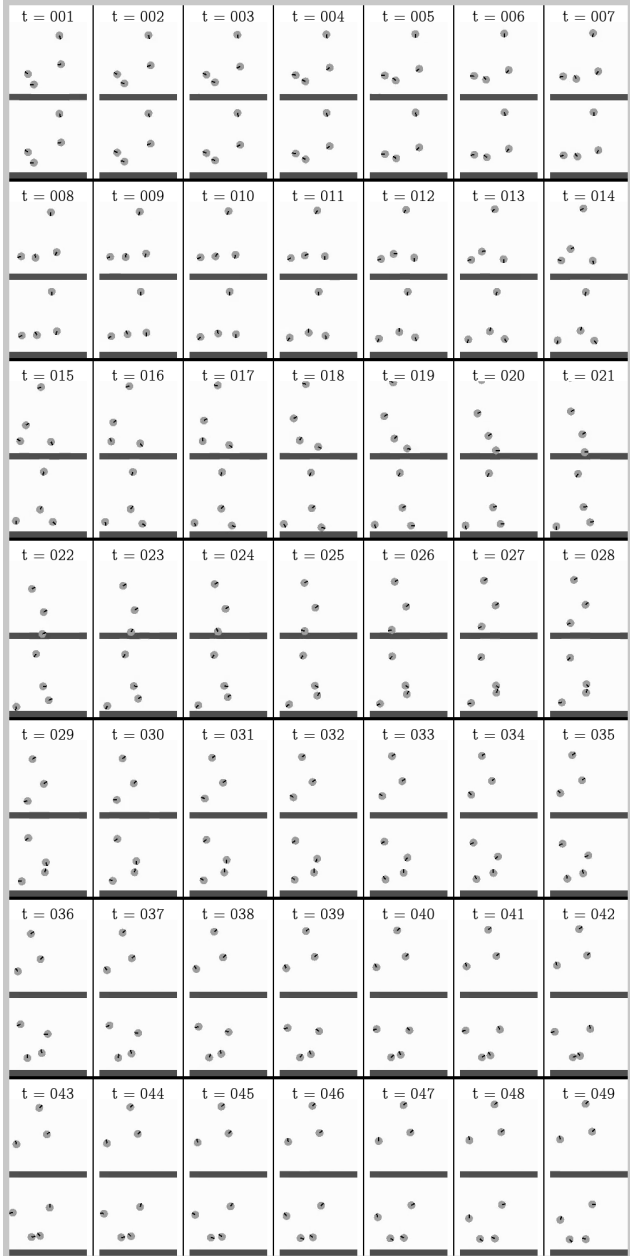


Figure 18. Example rollout using baseline transformer trained on 1000 episodes of 4 circles using sequence length 16. For each timestep, model prediction is shown in the top panel, and the ground truth environment simulation in the bottom panel.

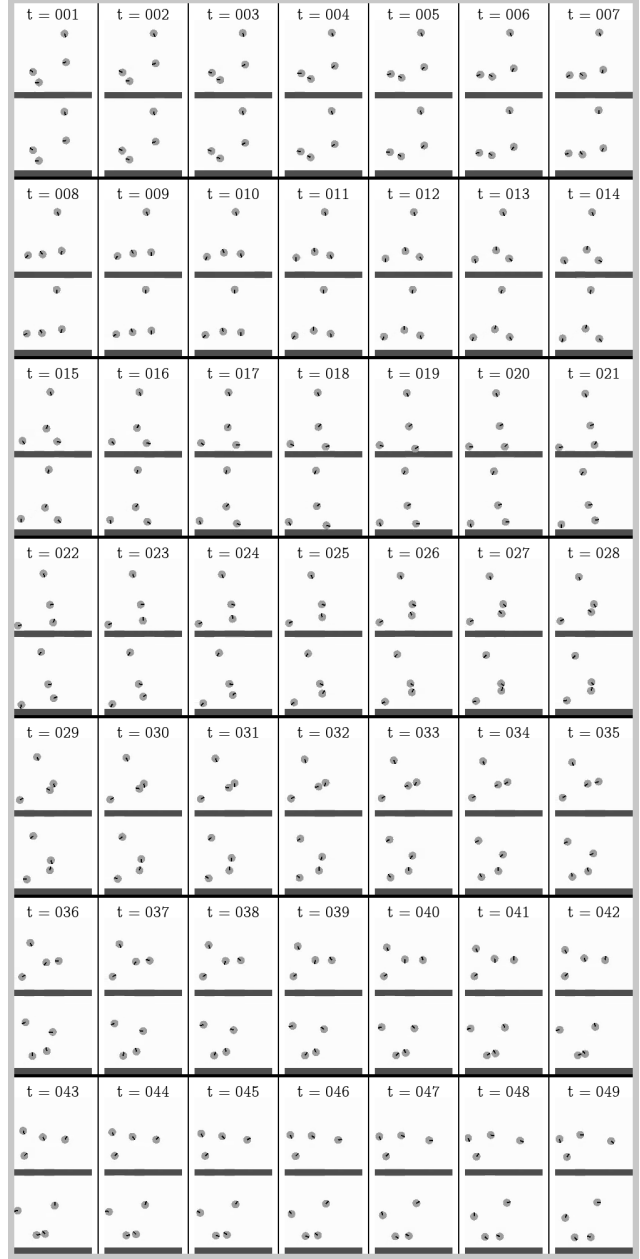


Figure 19. Example rollout using S-Ad-CliffordTransformer, using adjoint linear layers, trained on 1000 episodes of 4 circles using sequence length 16. For each timestep, model prediction is shown in the top panel, and the ground truth environment simulation in the bottom panel.

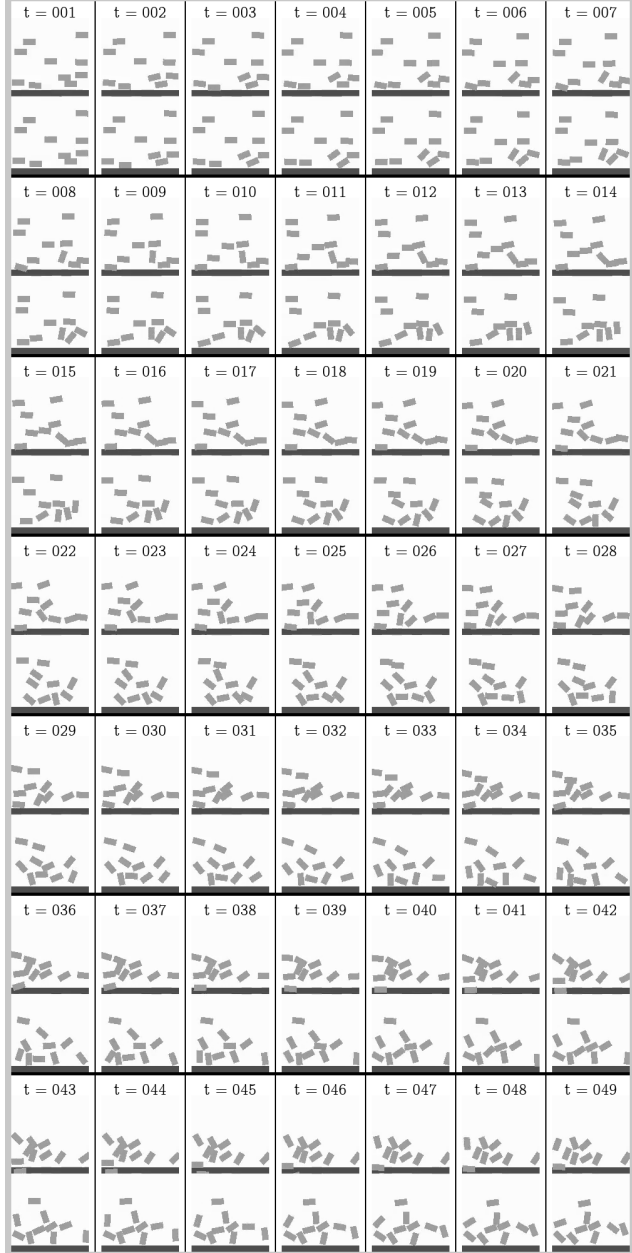


Figure 20. Example rollout using Equi-CliffordTransformer, trained on 1000 episodes of 10 rectangles using sequence length 2. For each timestep, model prediction is shown in the top panel, and the ground truth environment simulation in the bottom panel.

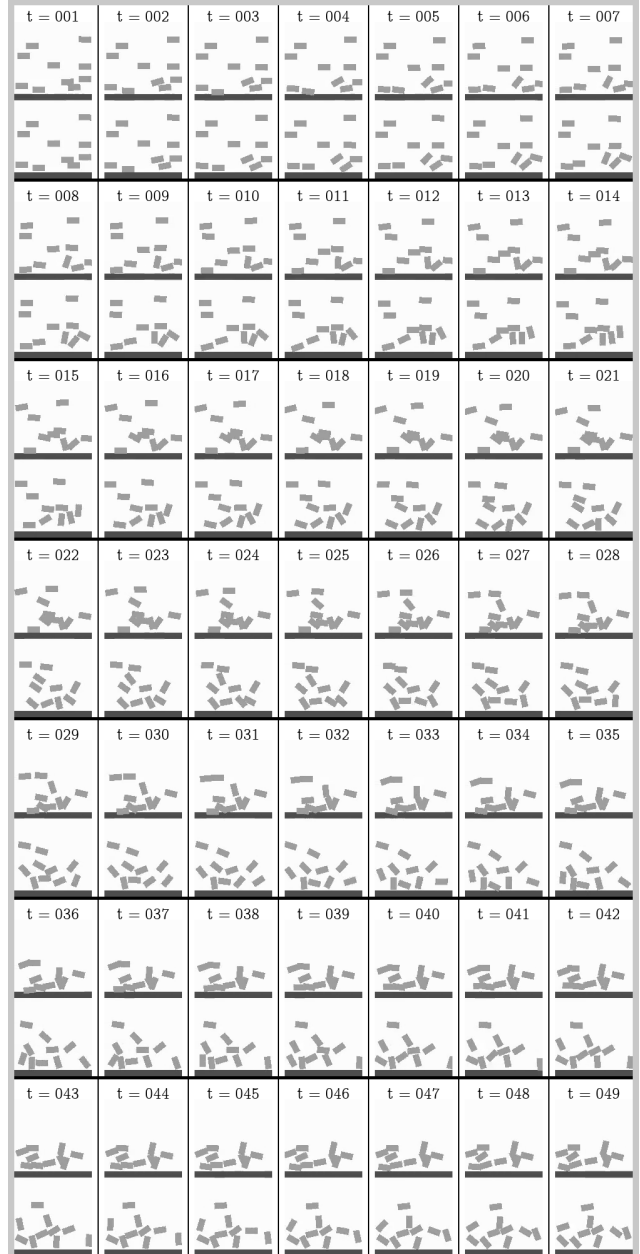


Figure 21. Example rollout using S-CliffordTransformer, trained on 1000 episodes of 10 rectangles using sequence length 2. For each timestep, model prediction is shown in the top panel, and the ground truth environment simulation in the bottom panel.



Figure 22. Example rollout using the baseline Transformer, trained on 1000 episodes of 10 rectangles using sequence length 2. For each timestep, model prediction is shown in the top panel, and the ground truth environment simulation in the bottom panel.